ACADEMIC PRESS

Available online at www.sciencedirect.com
SCIENCE DIRECT®

NeuroImage

NeuroImage 20 (2003) 1743–1755

www.elsevier.com/locate/ynimg

A neural mass model for MEG/EEG: coupling and neuronal dynamics

Olivier David* and Karl J. Friston

Wellcome Department of Imaging Neuroscience, Functional Imaging Laboratory, 12 Queen Square, London WC1N 3BG, UK

Received 21 February 2003; revised 18 July 2003; accepted 22 July 2003

Abstract

Although MEG/EEG signals are highly variable, systematic changes in distinct frequency bands are commonly encountered. These frequency-specific changes represent robust neural correlates of cognitive or perceptual processes (for example, alpha rhythms emerge on closing the eyes). However, their functional significance remains a matter of debate. Some of the mechanisms that generate these signals are known at the cellular level and rest on a balance of excitatory and inhibitory interactions within and between populations of neurons. The kinetics of the ensuing population dynamics determine the frequency of oscillations. In this work we extended the classical nonlinear lumped-parameter model of alpha rhythms, initially developed by Lopes da Silva and colleagues [Kybernetik 15 (1974) 27], to generate more complex dynamics. We show that the whole spectrum of MEG/EEG signals can be reproduced within the oscillatory regime of this model by simply changing the population kinetics. We used the model to examine the influence of coupling strength and propagation delay on the rhythms generated by coupled cortical areas. The main findings were that (1) coupling induces phase-locked activity, with a phase shift of 0 or π when the coupling is bidirectional, and (2) both coupling and propagation delay are critical determinants of the MEG/EEG spectrum. In forthcoming articles, we will use this model to (1) estimate how neuronal interactions are expressed in MEG/EEG oscillations and establish the construct validity of various indices of nonlinear coupling, and (2) generate event-related transients to derive physiologically informed basis functions for statistical modelling of average evoked responses.

1. Introduction

It is generally assumed that the signals measured in magnetoencephalography (MEG) and electroencephalography (EEG) can be decomposed into distinct frequency bands (delta: 1–4 Hz, theta: 4–8 Hz, alpha: 8–12 Hz, beta: 12–30 Hz, gamma: 30–70 Hz) (Nunez, 1981). These rhythms sometimes exhibit robust correlates of behavioural states but often with no obvious functional role. It is clear that MEG/EEG signals result mainly from extracellular current flow, associated with massively summed postsynaptic potentials in synchronously activated and vertically oriented neurons (dendritic activity of macro-columns of pyramidal cells in the cortical sheet). The exact neurophysiological mechanisms, which constrain this synchronisation to a given frequency band, remain obscure. However, the generation of oscillations appears to depend on interactions between inhibitory and excitatory populations, whose kinetics determine their oscillation frequency. This dependency suggests a modelling strategy could help to disclose the causes of different MEG/EEG rhythms and to characterise the neuronal processes underlying MEG/EEG activity.

There are several ways to model neural signals (Whittington et al., 2000a): either using a detailed model, in which it is difficult to determine the influence of each model parameter, or a simplified one, in which realism is sacrificed for a more parsimonious description of key mechanisms. The complexity of neural networks generating MEG/EEG signals is such that the second approach is usually more viable. This involves modelling neuronal activity with simplifying assumptions and empirical priors to emulate realistic signals. Neural mass models (Freeman, 1978; Lopes da Silva et al., 1974; Robinson et al., 2001; Stam et al., 1999; Valdes et al., 1999; Wendling et al., 2000) are based upon this approach. These models comprise macro-columns, or

* Corresponding author. Fax: +44-207-813-1420.
E-mail address: odavid@fil.ion.ucl.ac.uk (O. David).

1053-8119/$ – see front matter © 2003 Elsevier Inc. All rights reserved.
doi:10.1016/j.neuroimage.2003.07.015

even cortical areas, using only one or two state variables to represent the mean activity of the whole population. This procedure, sometimes referred to as a "mean-field approximation," is very efficient for determining the steady-state behaviour of neuronal systems, but its utility in a dynamic or nonstationary context is less established (Haskell et al., 2001). The majority of neural mass models of EEG responses have been designed to model alpha rhythms (Jansen and Rit, 1995; Lopes da Silva et al., 1974; Stam et al., 1999). Recent studies have emphasised that the kinetics of inhibitory populations have a key influence on the signals generated (Wendling et al., 2002). Specifically, it has been suggested that fast inhibition kinetics are needed to produce gamma-like activity (Jefferys et al., 1996). In fact, MEG/EEG signals depend upon the kinetics of both inhibitory and excitatory neural populations, and exhibit very complex dynamics because of the huge diversity and connectivity of cortical areas.

In this study we describe a simple neural mass model that can produce various rhythms ranging from delta to gamma, depending on the kinetics of the populations modelled. We start from the model of Jansen and Rit, (1995) using standard parameters to produce alpha activity in a single area. We then show that variation of excitatory and inhibitory kinetics, within a physiologically plausible range, can generate oscillatory activity in the delta, theta, alpha, beta, and gamma bands using the same model. Next, we assume that a cortical area comprises several resonant neuronal populations, characterised by different kinetics. We describe the particular case of two populations that underlie intrinsic alpha and gamma rhythms. In this dual-kinetic model, a single parameter controls the relative contribution of fast and slow populations, leading to a modulation of the rhythms produced. Finally, we address the coupling of two areas, with a particular focus on the dependence of cortical rhythms upon the strength of the coupling and upon the distance between cortical areas (modelled as a propagation delay). Using several sets of parameters, we show that this model can generate a wide variety of oscillations in the alpha, beta, and gamma bands that are characteristic of MEG/EEG signals.

The goal of this study is to introduce and characterise the behaviour of the model. This is the first component of a broader program that aims to (1) quantify the sensitivity of linear and nonlinear methods for the detection of long-range cortical interactions using MEG/EEG signals, and (2) model event-related dynamics and derive basis functions for statistical models of averaged evoked potentials/fields.

2. Neural mass models

MEG/EEG signals are generated by the massively synchronous dendritic activity of pyramidal cells. Modelling MEG/EEG signals is seldom tractable using realistic models, at the neuronal level, because of the complexity of real neural networks. Since the 1970s (Freeman, 1978; Lopes da Silva et al., 1974; Nunez, 1974; Wilson and Cowan, 1972) the preferred approach has been the use of neural mass models, i.e., models that describe the average activity with a small number of state variables. These states summarise the behaviour of millions of interacting neurons. Basically, these models use two conversion operations (Jirsa and Haken, 1997; Robinson et al., 2001): a wave-to-pulse operator at the soma of neurons, which is generally a static sigmoid function, and a linear pulse-to-wave conversion implemented at a synaptic level, within the ensemble. The first operator relates the mean firing rate to average postsynaptic depolarisation. This is assumed to be instantaneous. The second operator depends on synaptic kinetics and models the average postsynaptic response as a linear convolution of incoming spike rate. The shape of the convolution kernels embodies the synaptic and dendritic kinetics of the population.

We based our work on the Jansen model (Jansen and Rit, 1995), which is one of the simplest models that are established in the literature. First, we present this model and then make modifications that engender richer dynamics.

2.1. Models of a single area

2.1.1. Jansen's model

Jansen's model (Jansen and Rit, 1995) is based upon a previous lumped parameter model (Lopes da Silva et al., 1974). The basic idea behind these models is to make excitatory and inhibitory populations interact such that oscillations emerge. A cortical area, understood here as an ensemble of strongly interacting macro-columns, is modelled by a population of excitatory pyramidal cells, receiving (1) inhibitory and excitatory feedback from local (i.e., intrinsic) interneurons, and (2) excitatory input from neighbouring or remote (i.e., extrinsic) areas. Any extrinsic input is represented by a pulse density $p(t)$ (c.f. neuronal firing rate), which depends on time t. In this work $p(t)$ is modelled by a stochastic Gaussian process.

The evolution of the population dynamics rests on two operators. The first transforms the average density of presynaptic input $m(t)$ [that includes $p(t)$] arriving at the population into an average postsynaptic membrane potential (PSP) $v(t)$. This is modelled by the linear transformation

$$v = h \otimes m \tag{1}$$

where $\otimes$ denotes the convolution operator in the time domain and h is the impulse response or first-order kernel

$$h(t) = \begin{cases} H \dfrac{t}{\tau} \exp\left(-\dfrac{t}{\tau}\right) & t \geq 0 \\ 0 & t < 0 \end{cases} \tag{2}$$

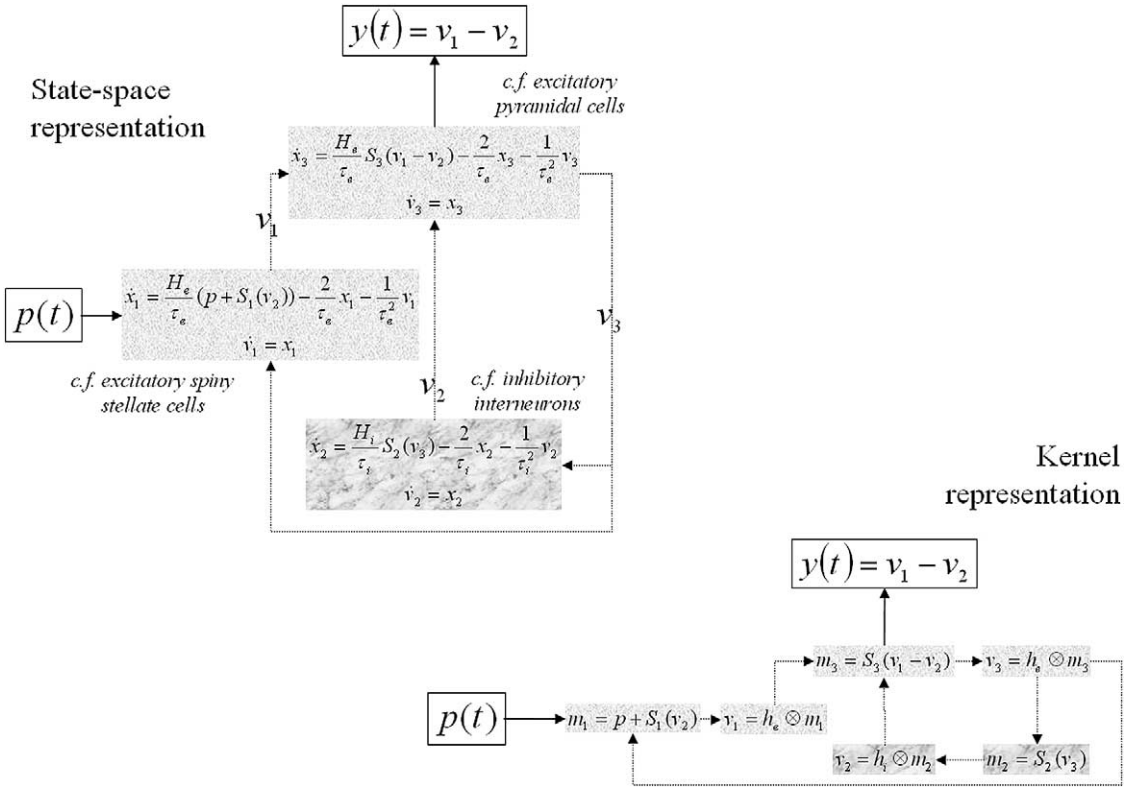

Fig. 1. Equivalent state-space and kernel representations of the Jansen neural mass model. Three different populations of neurons (excitatory pyramidal cells, excitatory stellate cells, and inhibitory interneurons) compose a cortical area. The extrinsic input *p* acts on excitatory spiny stellate cells. The MEG/EEG signal *y* is the dendritic depolarisation of excitatory pyramidal cells. The mean-field approximation describes the state of each neuronal population by the average membrane potential ν and mean firing rate *m*. The transformation from *m* to ν is described by the kinetic-dependent operator *h*, while the converse nonlinear transformation *S* is assumed to be sigmoid and instantaneous.

The excitatory (*e*) and inhibitory (*i*) kernels, h_e and h_i, respectively, are parameterised by $H_{e,i}$ and $\tau_{e,i}$ modelling specific properties of inhibition and excitation. The parameters $H_{e,i}$ tune the maximum amplitude of PSPs and $\tau_{e,i}$ are a lumped representation of the sum of the rate constants of passive membrane and other spatially distributed delays in the dendritic tree.

The second operator transforms the average membrane potential of the population into an average rate of action potentials fired by the neurons. This transformation is assumed to be instantaneous and is described by the sigmoid function

$$S_k(\nu) = \frac{c_k^1 e_0}{1 + \exp\left(r(\nu_0 - c_k^2 \nu)\right)} \tag{3}$$

for the *k*th subpopulation. $c_k^{1,2}$, e_0, r, and ν_0 are parameters that determine its shape (e.g., voltage sensitivity).

Interactions among the different subpopulations are characterised by constants $c_k^{1,2}$, which account for the intrinsic circuitry and the total number of synapses expressed by the subpopulation's interneurons and pyramidal cells. These constants can be estimated using anatomical information from the literature, as described by Jansen and Rit (1995). The model is summarised in Fig. 1 using both state-space and kernel representations. These representations are mathematically equivalent. We use the kernel representation to summarise the architecture of subsequent extensions below, but integrate the differential equations of the state-space form when simulating dynamics per se.

The MEG/EEG signal is assumed to be modelled by *y(t)*, the average depolarisation of pyramidal cells (Fig. 1). For the sake of simplicity, we ignore the observation equation, i.e., how *y(t)* is measured. This includes not only the effects of amplifiers (which are an additional band-pass filter), but also the MEG/EEG lead fields that indicate the spatial distribution of the electromagnetic field in the head using Maxwell equations and suitable head models (Baillet et al., 2001). For given synaptic responses *h* and sigmoid functions *S*, the Jansen model can produce a large variety of MEG/EEG-like waveforms (broad-band noise, epileptic-like activity) and alpha rhythms (Jansen and Rit, 1995; Wendling et al., 2000). In this study we were interested in oscillatory signals. Consequently, we consider the Jansen model in its oscillatory regime, which is obtained using the set of parameters shown in Table 1. As described by Jansen and Rit (1995), these produce a well-defined alpha activity. However, a modification of the parameters can lead to the generation of faster and slower oscillations as shown next.

Table 1
Physiological interpretation and standard values of model parameters (adapted from Wendling et al., 2000)

Parameter	Physiological interpretation	Standard value
$H_{e,i}$	Average synaptic gain	$H_e = 3.25$ mV, $H_i = 22$ mV
$\tau_{e,i}$	Membrane average time constant and dendritic tree average time delays	$\tau_e = 10$ ms, $\tau_i = 20$ ms
$c_1^{1,2}$	Average number of synaptic contacts in the excitatory feedback loop	$c_1^1 = c$, $c_1^2 = 0.8c$ $c = 135$
$c_2^{1,2}$	Average number of synaptic contacts in the inhibitory feedback loop	$c_2^1 = c_2^2 = 0.25c$
$c_3^{1,2}$		$c_3^1 = c_3^2 = 1$
ν_0, e_0, r	Parameters of the nonlinear sigmoid function	$\nu_0 = 6$ mV, $e_0 = 5$ s^{-1} $r = 0.56$ mV^{-1}

2.1.2. Extension of the Jansen model to multiple populations

In the oscillatory mode, the model described above produces a narrow-band signal, the frequency of which depends on the neuronal time constants adopted in h. To reproduce richer oscillatory MEG/EEG signals (including broad and multi-band spectra), we now extend the Jansen model. We assume that the Jansen model is sufficient to reproduce the dynamics of a single cell assembly. To capture the diversity of neuronal networks within the thalamocortical system (Steriade, 2001), we model a cortical area with N populations, deployed in parallel, with different kinetics for each subpopulation (excitatory and inhibitory). As shown in Fig. 2, the extended model derives from the Jansen model in the simplest way by creating multiple subpopulations with kernels $\lfloor h_{e,i}^1, \ldots, h_{e,i}^N \rfloor$ that embody different kinetics. The implicit assumptions are that (1) the different ensembles express the same cytoarchitectonic structure (identical constants $c_k^{1,2}$), and (2) have the same inputs (on average). The parameters w^n, $n = [1, \ldots, N]$, bounded between 0 and 1, adjust the relative proportion of each population in the cortical area. They respect the constraint $\sum_{n=1}^{N} w^n = 1$ and can be time-dependent, modelling short-term synaptic plasticity that can occur, for instance, during attentional modulation. In the next subsection we consider how the model can be further generalised to multiple areas.

2.2. Models of multiple areas

Neurophysiological studies have shown that cortical outputs to distant targets are exclusively excitatory. Moreover, experimental evidence suggests that MEG/EEG activity is generated by strongly coupled but remote cortical areas (David et al., 2002; Engel et al., 2001; Rodriguez et al., 1999; Varela et al., 2001). Fortunately, modelling excitatory coupling is straightforward using the Jansen model and

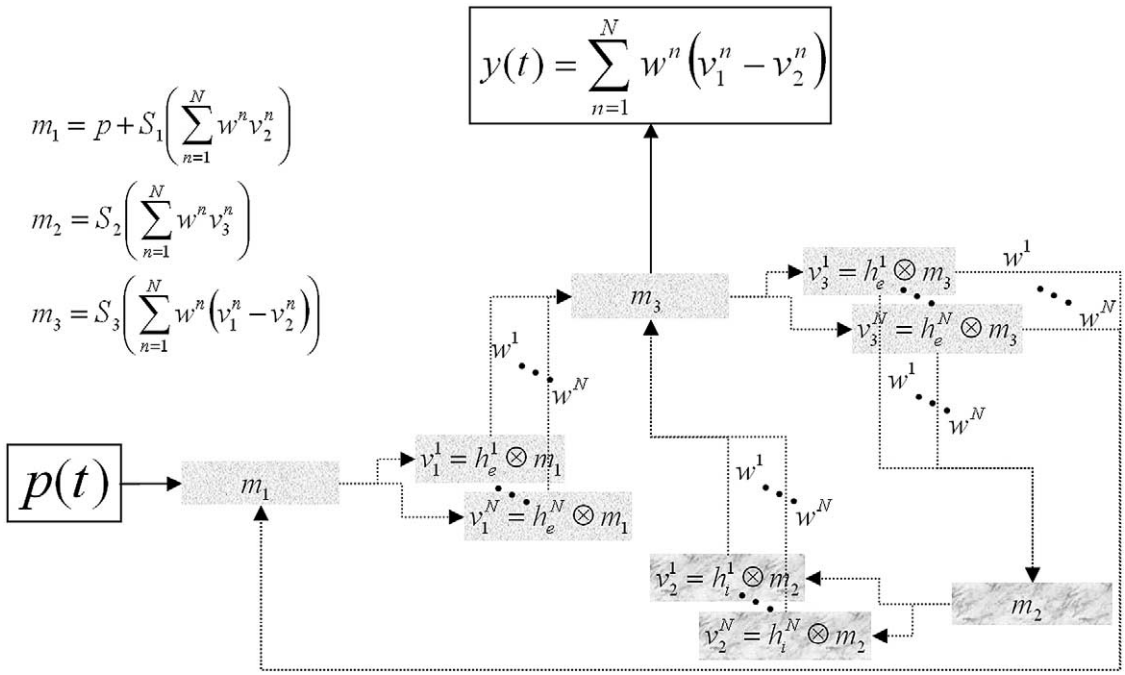

Fig. 2. The generalisation of the Jansen model is obtained by splitting the linear operators $h_{e,i}$ into N parts $\lfloor h_{e,i}^1, \ldots, h_{e,i}^N \rfloor$, which represent N populations of different kinetics. The parameters w^n (between 0 and 1) tune the contribution of each population and respect $\sum_{n=1}^{N} w^n = 1$.

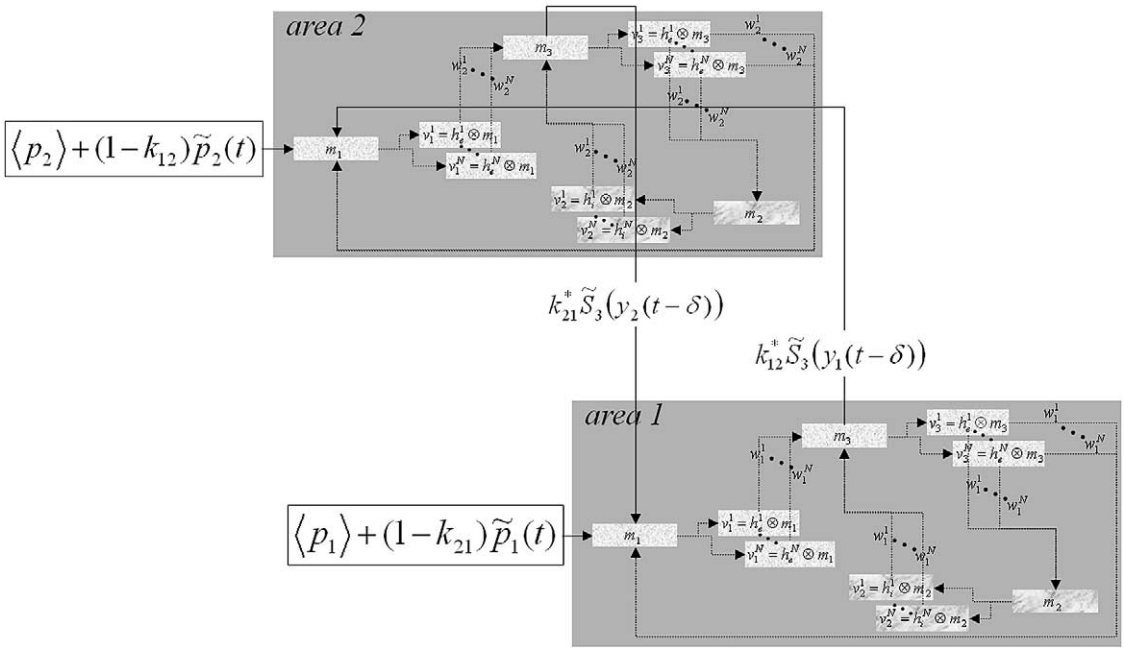

Fig. 3. Coupling of two areas: the mean firing rate of pyramidal cells $S_3(y)$ of one area is connected to the input of the other area after applying a propagation delay δ and coupling coefficients k_{12} and k_{21} (bounded between 0 and 1), which quantify the contribution of one area to the input of the other. Some variables are expressed as deviations from their expectation (for instance $p_{1,2}(t) = \langle p_{1,2} \rangle + \tilde{p}_{1,2}(t)$).

some consequences of excitatory to excitatory coupling have been described already (Jansen and Rit, 1995; Wendling et al., 2000).

In this section we consider two areas, each modelled as above, and coupled by excitatory connections. To isolate the effect of coupling, on oscillatory dynamics, we ensured that the equilibrium activity of each population was maintained, i.e., the mean and variance of presynaptic input to each population did not change with coupling. This was achieved by scaling the presynaptic component from the other area relative to the extrinsic (noise) input for each set of coupling parameters. An interpretation of this constraint is that the coupling value represents the proportion of presynaptic input attributable to the source area. This constraint renders coupling operationally equivalent to the "contribution" of one area to another (Friston et al., 1997).

The coupling strategy is shown in Fig. 3, where the presynaptic inputs enter as deviations from their expectation

$$p(t) = \langle p \rangle + \tilde{p}(t) \tag{4}$$

$$S_3(y(t-\delta)) = \langle S_3(y) \rangle + \tilde{S}_3(y(t-\delta))$$

and $\langle \quad \rangle$ is the average over time. This ensures mean input is conserved for different coupling parameters. The coupling disposition between two areas means that the output $\tilde{S}_3(y_1)$ of area 1 contributes to the input of area 2 in proportion to k_{12}^{*}, while the amplitude of extrinsic noise to area 2 decreases by $1 - k_{12}$. The directed coupling coefficient k_{12} is specified between 0 and 1 and k_{12}^{*} is adjusted to ensure that the standard deviation (σ) of total presynaptic input $\sigma_{(1-k_{12})\tilde{p}_2 + K_{12}^{*}\tilde{S}_3(y_1)}$ is conserved at σ_{p2}. Noting that $\langle \tilde{p}_2 \tilde{S}_3(y_1) \rangle = 0$, it can be rewritten in terms of variance and the expression of k_{12}^{*} derived

$$k_{12}^{*2}\sigma_{S_3(y_1)}^2 + (1-k_{12})^2\sigma_{p_2}^2 = \sigma_{p_2}^2 \Rightarrow$$

$$k_{12}^{*} = \frac{\sigma_{p_2}\sqrt{2k_{12} - k_{12}^2}}{\sigma_{S_3(y_1)}} \tag{5}$$

Similarly for k_{21}^{*}. A precise estimation of the coupling parameters is important because slight overestimations lead to exponential growth of oscillations and saturation, due to the sigmoid functions of the model. Practically, the values of k_{12}^{*} were updated at each time step using the sample variance of $S_3(y_1)$ over previous time steps (similarly for k_{21}^{*}). This approach converged for every set of parameters, after some transient that was removed before further analysis.

This scheme allowed us to specify a coupling coefficient k_{12} bounded between 0 (no coupling) and 1 (no extrinsic input) without changing the overall inputs to any area. In other words, for a small coupling between areas, most input variance, for a given area, is attributable to extrinsic background activity (white noise). A larger coupling (i.e., contribution) induces a relatively stronger influence of the driving area.

3. Dynamic properties of simulated signals

For each simulation described below, the differential equations were solved numerically using a second order

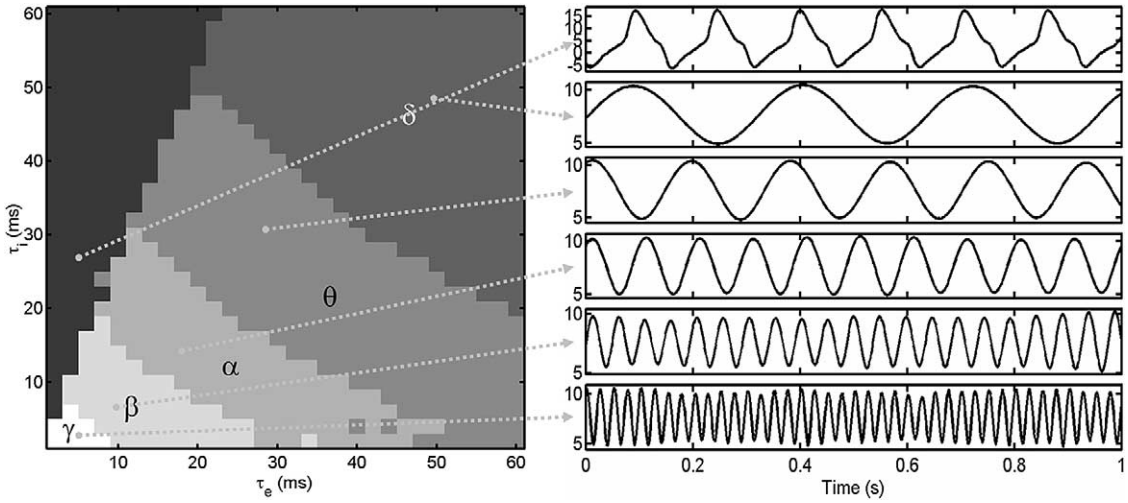

Fig. 4. Rhythms generated using the Jansen model for different synaptic kinetics [τ_e, τ_i]. On the left-hand side, a phase-space representation was obtained by measuring the peak frequency of oscillations after averaging over 10 realisations. The greyscale codes different frequency bands [delta (1–4 Hz), theta (4–8 Hz), alpha (8–12 Hz), beta (12–30 Hz), gamma (>30 Hz)]. The black area is a zone of hypersignal not representative of normal activity. Examples of simulated signals are shown on the right-hand side.

Runge-Kutta algorithm (a fourth-fifth order Runge-Kutta method gave similar results). As it is known that this type of algorithm is not optimal for stochastic differential equations, we compared the simulated signals with those generated using a second order stochastic Runge-Kutta algorithm (Honeycutt, 1992). There were no qualitative differences between the two integration schemes. The time resolution was 1 ms. The extrinsic input *p(t)* was a Gaussian innovation ($\langle p \rangle = 220$, $\sigma_p = 22$) simulating input from unspecified cortical and subcortical areas.

3.1. Neural kinetics and oscillations in the Jansen model

The typical parameters, proposed by Jansen and Rit (1995), enable the generation of alpha rhythms. To investigate which other rhythms emerge, using physiologically plausible values of average membrane time constants and time delays, we varied the values of $\tau_{e,i}$. To ensure oscillatory behaviour, the ratio $H_{e,i}/\tau_{e,i}$ was held constant. We used the ratio shown in Table 1 and adjusted the value of $H_{e,i}$ according to the values of $\tau_{e,i}$.

The parameters $\tau_{e,i}$ varied from 2 to 60 ms with a step size of 2 ms. Simulated signals were of 1-s duration. Fig. 4 summarises the results of these simulations. For each combination of $\tau_{e,i}$, we first checked whether signals exhibited a quasi-sinusoidal activity or saturated hyperactivity. In the case of quasi-sinusoidal activity, the peak frequency of the oscillations was measured and the dynamics were assigned to a MEG/EEG band. The results of these classifications are shown in Fig. 4. For each of the six domains of Fig. 4, a typical signal is shown. It appears that adjusting the kinetic properties of neural subpopulations in the Jansen model engenders oscillatory signals from the delta to the gamma band. However, one must note that the results in Fig. 4 depend critically upon the value of the parameters $c_k^{1,2}$ which determine the oscillatory frequency range.

3.2. Oscillations in the generalised Jansen model

For the sake of simplicity, we consider only the generalised model in the particular case of two populations with different kinetics (a dual-kinetics model). We specified the parameters so that the resonant frequency of the slow population fell in the alpha band, according to the Jansen model ($\tau_e^1 = 10.8$ ms; $\tau_i^1 = 22$ ms). We tuned the kinetics of the fast population ($\tau_e^2 = 4.6$ ms; $\tau_i^2 = 2.9$ ms) so that it resonated in the gamma band, emulating local neuronal pacemakers (Jefferys et al., 1996). As noted above, the relative size of the two populations is tuned by the parameters w^1 and w^2, which lie between 0 and 1 where $w^1 + w^2 = 1$. For simplicity, we define $w = w^1$ and consider this single ratio parameter, given that $w^2 = 1 - w$. This configuration was chosen to explore the alpha, beta, and gamma dynamics using a minimal model as shown below. When reproducing real data, the model configuration can be changed to emulate observed oscillations.

Fig. 5 shows the influence of *w* on simulated dynamics. For several values of *w*, signals were simulated with and without extrinsic input. On the right-hand side, the time courses and their spectra averaged over 10 trials to attenuate the contribution from stochastic innovations. When $w = 0$ or $w = 1$, oscillations are produced even without extrinsic input, as shown on the left-hand side. For intermediate values of *w*, oscillations are driven stochastically by the input (i.e., no oscillatory dynamics in the absence of input). Variation of *w* transforms the spectrum of simulated MEG/EEG signals from alpha to gamma bands. It is interesting to note that the spectrum is never bimodal, even when both

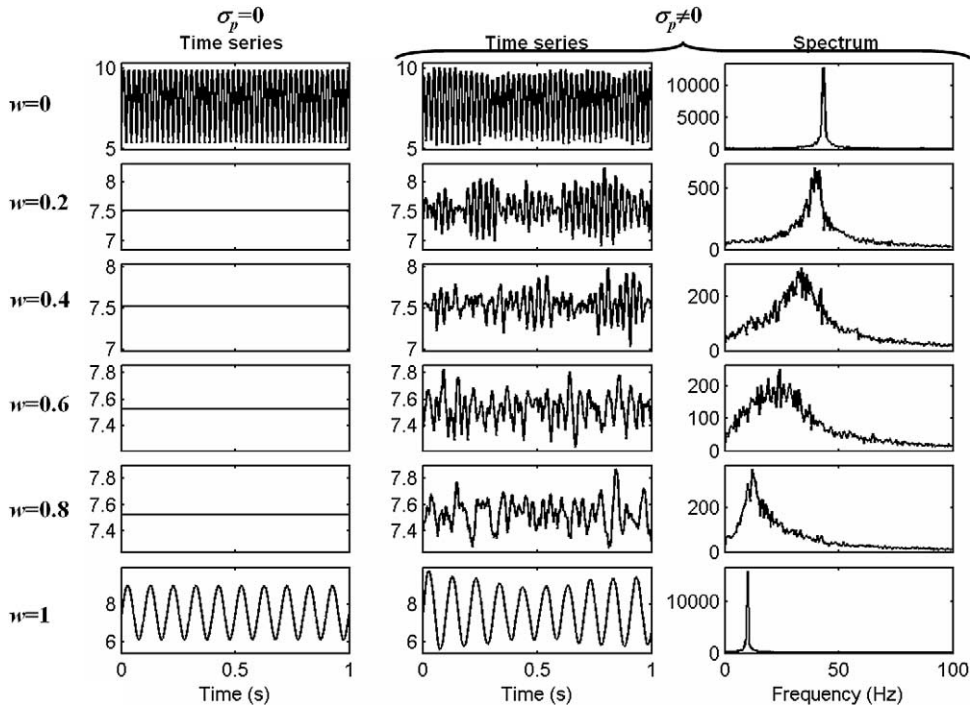

Fig. 5. Dependence of oscillations upon the parameter w used in the dual-kinetic model in order to tune the relative contribution of slow (~10 Hz) and fast (~43 Hz) kinetics. On the right-hand side, the time courses and their spectra averaged over 10 trials are shown when extrinsic input is applied ($\sigma_p \neq 0$). When $w = 0$ or $w = 1$, oscillations are produced even without extrinsic input ($\sigma_p = 0$) as shown on the left-hand side. For intermediate values of w, oscillations are driven stochastically by the input noise.

populations contribute substantially, and most characteristic MEG/EEG spectra are obtained when w falls between 0.8 and 1.

3.3. Coupling and simulated dynamics

In this section we restrict our simulations to a model composed of two areas using the dual-kinetics model of the previous subsection and investigate the influence of coupling strength and propagation delay on the rhythms generated. A propagation delay δ of 10 ms was assumed. As the model allows either unidirectional or bidirectional coupling, we considered both possibilities. For each parameter configuration, signals were generated for 20 different realisations of extrinsic noise $p_{1,2}(t)$. To look at the effect of coupling on oscillations, we computed the spectra of signals and their coherence function to identify frequency bands that contain interactions.

3.3.1. Identical areas

First, we investigated the influence of coupling between two identical areas. To generate characteristic MEG/EEG signals, the parameters w_1 and w_2 corresponding to areas 1 and 2 respectively, were set to 0.8 (see Fig. 5).

First, area 1 was connected so as to drive area 2 by setting k_{21} to 0. Meanwhile k_{12} was set to either 0 or 0.5. Fig. 6 shows simulated signals, and the ensuing spectra and coherence function averaged over trials. With this unidirectional coupling, the spectrum of the driven area became mildly more frequency specific and the coherence increased. We observed a systematic delay of 18 ms between the signals in area 1 and 2, as indexed by the maximum of the cross-correlation function. This time delay was independent of the strength of the coupling and can be decomposed into the propagation delay (10 ms) and a synaptic delay (8 ms).

Second, bidirectional coupling was simulated by setting k_{12} equal to k_{21}. The results are shown in Fig. 7. The consequence of a bidirectional coupling was a phase-locking of well-defined oscillations as reflected in the very high coherence in two frequency bands, with a phase shift equal to 0 (in this simulation). In fact, as shown below, the relative phase between oscillations depends mostly upon the propagation delay and is equal to either 0 or π.

3.3.2. Areas with different kinetics

So far we have assumed that brain areas have the same composition of fast and slow neuronal populations (modelled by the parameter w). However, this mixture depends upon the brain structures involved. For instance, gamma rhythms may be more readily generated by the hippocampus (Whittington et al., 2000b) relative to some other areas. We investigated the scenario in which a fast oscillatory area ($w_1 = 0.2$), such as the hippocampus, is coupled to a slower area ($w_2 = 0.8$), say in a cortical area. The results shown below were obtained when the fast area drives the slow area or

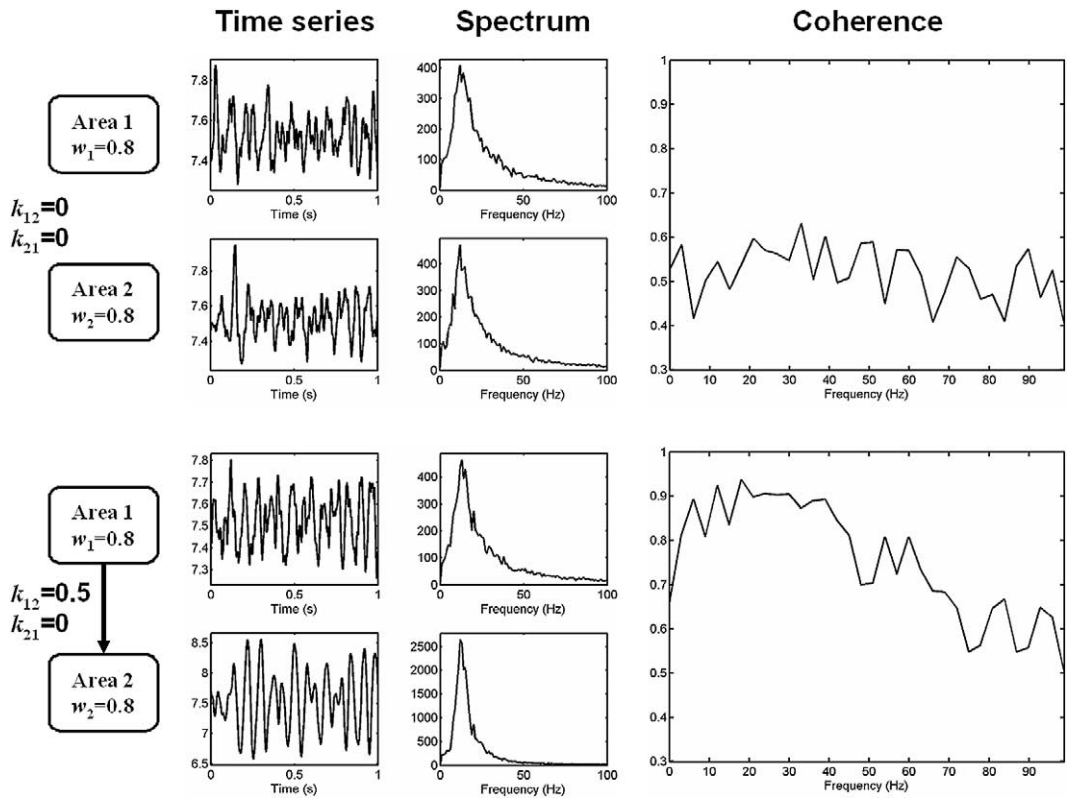

Fig. 6. Unidirectional coupling of two identical areas ($w_1 = w_2 = 0.8$, $\delta = 10$ ms). The top of the panel shows signals and their coherence when no coupling is applied. When unidirectional coupling is applied (area 1 drives area 2 on the bottom of the panel), the spectrum of area 2 gets narrower and coherence increases indicating a phase-locking of activities at the frequencies of oscillations. Because of the unidirectional coupling, the activity of area 2 is delayed in relation to area 1.

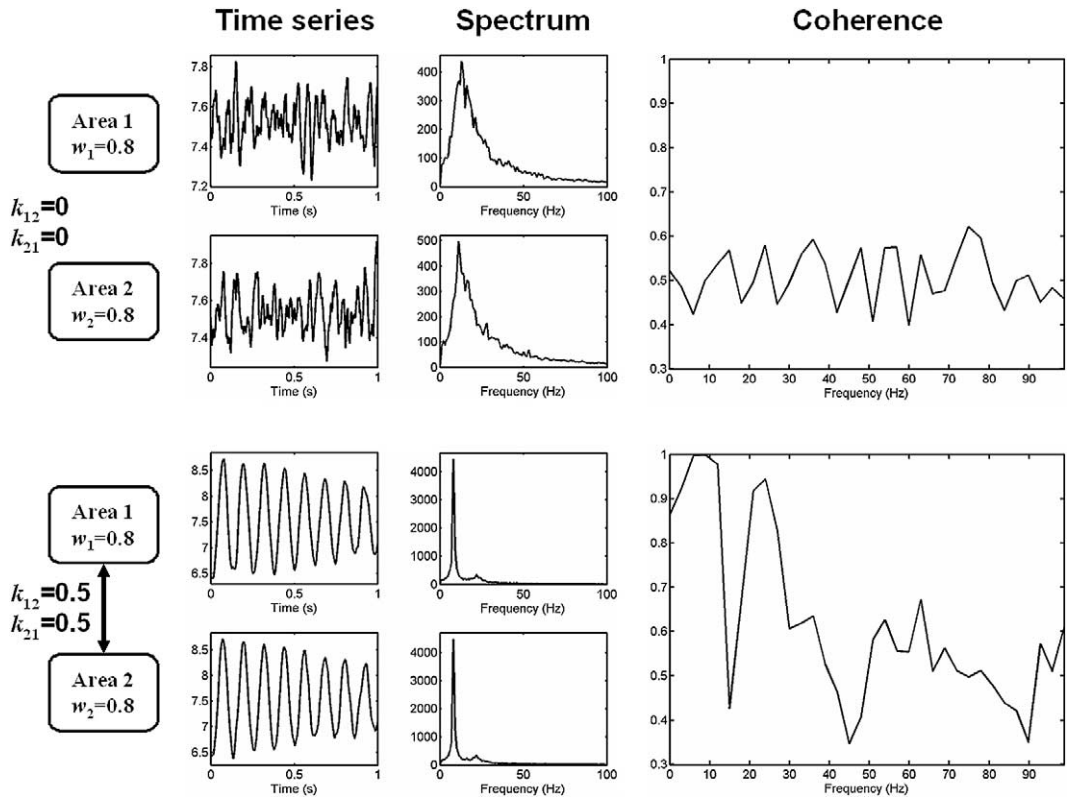

Fig. 7. Bidirectional coupling of two identical areas ($w_1 = w_2 = 0.8$, $k_{12} = k_{21}$, $\delta = 10$ ms). The top of the panel shows signals and their coherence when no coupling is applied. When bidirectional coupling is applied (bottom of the panel), the both spectra get very peaky, with one or two main frequencies of oscillations depending on the value of δ (Fig. 10). Moreover, the oscillations are in phase or antiphase, thus the coherence increases in the frequency bands of interaction.

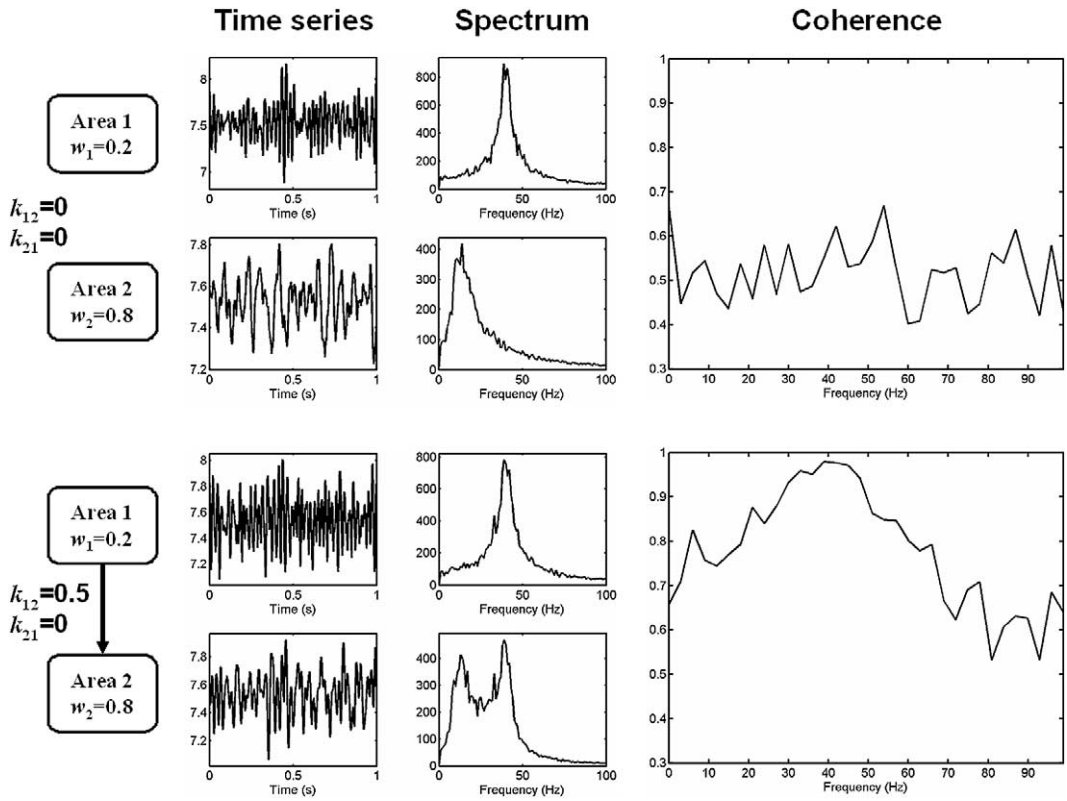

Fig. 8. Unidirectional coupling of two different areas ($w_1 = 0.2$, $w_2 = 0.8$, $\delta = 10$ ms). The faster area (area 1) drives area 2 ($k_{21} = 0$). The coupling makes appear fast rhythms in area 2 with no change in its intrinsic oscillations (slow rhythms). The coherence function increases mostly in the frequency band of area 1.

when the two areas are reciprocally coupled. Except for the change to w_1, the simulation parameters were the same as in the previous section.

Fig. 8 shows the results of simulations when the fast area drives the slow area (unidirectional coupling). A consequence of coupling is the emergence, in the slow area, of the fast rhythms expressed in the driving area. There is no modification of the slow oscillations intrinsic to the driven area but an increase of the coherence in the upper frequency band. As shown in Fig. 9, there is again a dramatic difference between rhythms generated using uni- and bidirectional coupling.

3.3.3. The influence of propagation delay and coupling strength

There are several lines of experimental evidence that suggest the distance between areas is negatively correlated within the frequency of some oscillations in the EEG (Nunez, 2000; von Stein and Sarnthein, 2000). We investigated this, using our model, by varying the propagation delay δ from 5 to 40 ms with 5-ms steps. Meanwhile the coupling strength $k = k_{12} = k_{21}$ was varied from 0.1 to 0.9 with a step size of 0.1. The architecture comprised two identical dual-kinetic areas with $w_1 = w_2 = 0.8$ that were reciprocally coupled.

For each set of parameters $[k,\delta]$, 10 realisations were obtained. Results are summarised in Fig. 10. A map of the frequency f_0 corresponding to the maximal peak of the average spectrum is shown: f_0 depends largely on the propagation delay δ and less on the coupling strength k. The average relative phase $\Phi_1 - \Phi_2$ at the frequency f_0 is either equal to 0 or π depending on the value of δ for strong coupling. Exemplar signals, obtained for $k = 0.1$ and 0.9 are shown. For $k = 0.1$ and large values of δ (>15 ms), the spectrum is unimodal and f_0 decreases with δ. However, within a small range of δ the spectra are bimodal, exhibiting peaks in alpha and beta bands. Increasing the coupling leads to quasi-sinusoidal activity.

In summary, a reciprocal coupling is characterised by well-defined oscillatory signals in phase or antiphase, even in the context of a large propagation delay. These findings agree with the experimental evidence of zero-lag synchronisation among remote cortical areas of spiking activity in awake animals (Chawla et al., 2001; Roelfsema et al., 1997). The relationship between the MEG/EEG spectrum and the distance between coupled areas is substantial. This supports the notion that propagation delay is a critical parameter in the genesis of frequency-specific interactions among cortical regions.

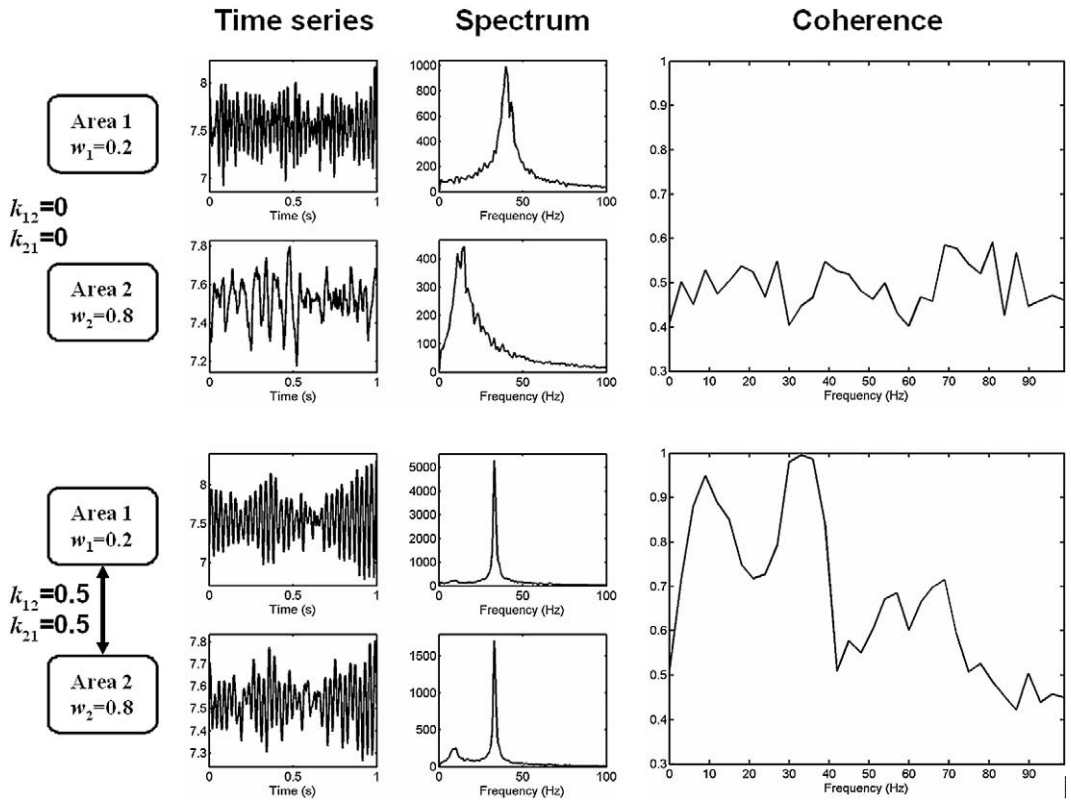

Fig. 9. Bidirectional coupling of two different areas ($w_1 = 0.2$, $w_2 = 0.8$, $k_{12} = k_{21}$, $\delta = 10$ ms). The spectra on the right are modified by the coupling (two well-defined frequency bands). The coherence function shows that the oscillations are phase-locked within each frequency band.

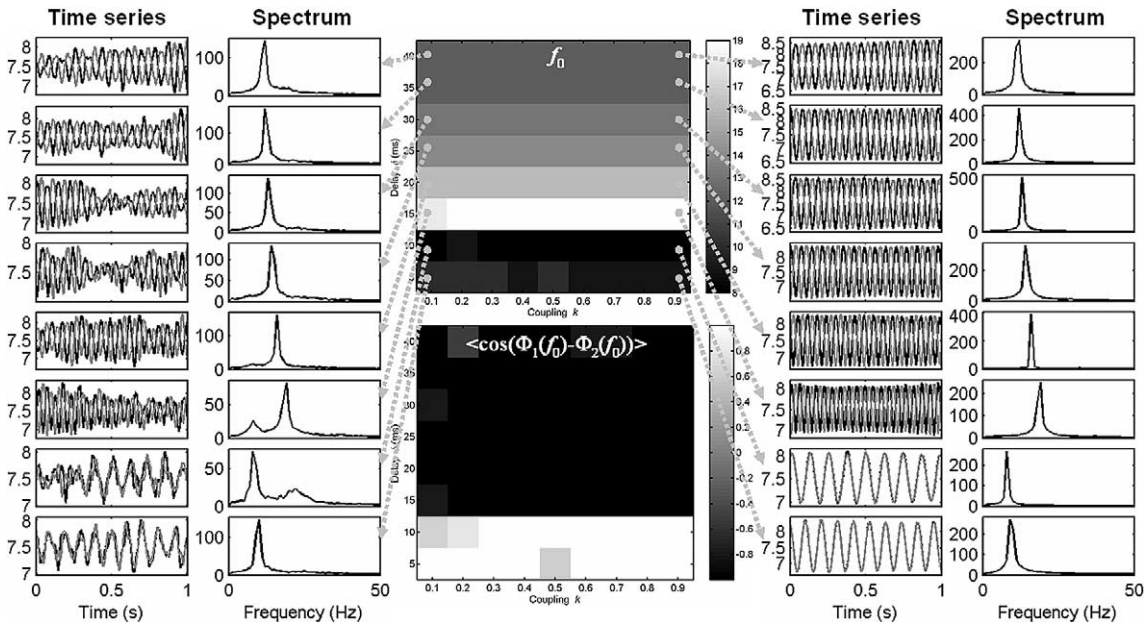

Fig. 10. Influence of the propagation delay and coupling strength upon oscillations of two mutually coupled identical areas ($w_1 = w_2 = 0.8$). For each set of parameters [k, δ], 10 realisations were performed. Top centre: a map of the frequency f_0 corresponding to the maximal peak of the average spectrum is shown: f_0 depends largely on the propagation delay δ and less on the coupling strength k. Bottom center: the average relative phase $\Phi_1 - \Phi_2$ at the frequency f_0 is either equal to 0 or π depending on the value of δ for strong coupling. Exemplar signals obtained for $k = 0.1$ and 0.9 are shown. For $k = 0.1$ and large values of δ (>15 ms), the spectrum is unimodal and f_0 decreases with δ. However, within a small range of δ the spectra are bimodal exhibiting peaks in alpha and beta bands. Increasing the coupling yields to quasi-sinusoidal activity.

4. Discussion

Neural mass models afford a straightforward approach to modelling the activity of populations of neurons. Their main assumption is that the state of the population can be approximated using very few state variables (generally limited to mean membrane currents, potentials, and firing rates). Given a macroscopic architecture, describing the overall connectivity (1) between populations of a given cortical area, and (2) between different cortical areas, it is possible to simulate the steady-state dynamics of the system or even the transient response to a perturbation of extrinsic input or connectivity. Consequently, neural mass models are useful to describe and predict the macroscopic electrical activity of the brain. Since the early 1970s, they have been used to address several important issues, e.g., alpha rhythms (Lopes da Silva et al., 1997), olfactory responses (Freeman, 1987), and focal attention (Suffczynski et al., 2001). They are now being introduced into neuroimaging to understand the underlying neuronal mechanisms of fMRI and PET data (Almeida and Stetter, 2002; Aubert and Costalat, 2002; Horwitz and Tagamets, 1999).

Despite their relative simplicity, neural mass models can exhibit complex dynamical behaviour reminiscent of the real brain. In this study we have shown that physiologically plausible synaptic kinetics lead to the emergence of oscillatory MEG/EEG-like signals covering the range of theta to gamma bands (Fig. 4). To emulate more complex oscillatory MEG/EEG dynamics, we have proposed a generalisation of the Jansen model that incorporates several distinct neural populations that resonate at different frequencies. Changing the composition of these populations induces a modulation of the spectrum of simulated MEG/EEG signals (Fig. 5).

We have investigated the consequence of coupling two remote cortical areas. It appears that the rhythms generated depend critically upon both the strength of the coupling and the propagation delay. As the coupling directly modulates the contribution of one area to another, the spectrum of the driven area, in the case of a unidirectional coupling, is obviously a mixture of the source and target spectra (Figs. 6 and 8). More interestingly, a bidirectional coupling engenders more marked modifications of the MEG/EEG spectrum that can include strong oscillatory activity (Figs. 7, 9, and 10). Bidirectional coupling is important because of the high proportion of reciprocal connections in the brain. The most robust consequence of coupling is phase synchronisation of remote oscillations. In the case of a bidirectional coupling, this phase-locking appeared to be equal to either 0 or π, depending upon the propagation delay (the phase-shift reflects the propagation delay if only unidirectional coupling is considered).

An important issue, which has not been addressed in this study, is how the model can be used to fit real data. The idea here is to treat the model as a forward or generative model of observed signals and estimate the model parameters given observations. The first step is to specify a network architecture (number of areas and how they are connected) with a small number of populations per area. For instance, for standard awake MEG/EEG recordings, three populations with intrinsic oscillations in the theta, alpha, and gamma bands may be sufficient to reproduce a large variety of spectra. Conditional estimates of the coupling and population composition parameters could, in principle, be obtained using procedures such as those proposed by Valdes et al. (1999) using measured data. See also Robinson et al. (2001); Friston (2002) and Friston et al. (2002).

Obviously neural mass models do not describe exactly how neural signals interact. These models represent a summary of underlying neurophysiological processes that cannot be modelled in complete detail because of their complexity. In particular, the model we used does not accommodate explicitly subcortical structures such as the reticular nuclei of the thalamus, which is thought to be involved in the genesis delta and alpha oscillations of the EEG (Steriade, 2001; Lumer et al., 1997). Despite these limitations, neural mass models are useful in helping to understand some macroscopic properties of MEG/EEG signals, such as nonlinearities (Stam et al., 1999) and coupling characteristics (Wendling et al., 2000). They can also be used to reconstruct a posteriori the scenario of inhibition/excitation balance during epileptic seizures (Wendling et al., 2002). Moreover, fitting simple models to actual MEG/EEG data, as described above, allows one to empirically determine likely ranges for some important physiological parameters (e.g., Robinson et al., 2001; Valdes et al., 1999).

In a forthcoming study we investigate the sensitivity of measures of regional interdependencies in MEG/EEG data, illustrating an important practical use of neural mass models. It is known that some interactions among cortical areas are reflected in MEG/EEG signals. In the literature, numerous analytic tools are used to reveal these statistical dependencies. These methods include cross-correlation, coherence (Clifford Carter, 1987), mutual information (Roulston, 1999), nonlinear correlation (Pijn et al., 1992), nonlinear interdependencies or generalised synchronisation (Arnhold et al., 1999), neural complexity (Tononi et al., 1994), synchronisation likelihood (Stam and van Dijk, 2002), and phase synchronisation (Lachaux et al., 1999; Tass et al., 1998). These interdependencies are established in a way that allows one to make inferences about the nature of the coupling. However, it is not clear which aspects of neuronal interactions are critical for causing the frequency-specific linear and nonlinear dependencies observed. Using the model described in this study, we will estimate how synaptic activity and neuronal interactions are expressed in MEG/EEG data and establish the construct validity of various indices of nonlinear coupling.

Another important application of neural mass models is the study of event-related dynamics. Indeed events can be simulated easily by using impulses of extrinsic input $p(t)$ to cortical areas. The consequence of such input is a transient

modulation of oscillations on which is superimposed the system's impulse response. This impulse response can be estimated by averaging single trials. Simulating evoked transients of this sort allows one to derive physiologically motivated basis functions that can be used for statistical inferences of averaged evoked potentials/fields in the framework of the general linear model as already used for fMRI (Frackowiak et al., 1997). This device could potentially bring the analysis of MEG/EEG data into a common PET/fMRI/MEG/EEG framework.

Acknowledgment

This work was supported by The Wellcome Trust.

References

Almeida, R., Stetter, M., 2002. Modeling the link between functional imaging and neuronal activity: synaptic metabolic demand and spike rates. NeuroImage 17, 1065–1079.

Arnhold, J., Grassberger, P., Lehnertz, K., Elger, C.E., 1999. A robust method for detecting interdependences: application to intracranially recorded EEG. Physica D 134, 419–430.

Aubert, A., Costalat, R., 2002. A model of the coupling between brain electrical activity, metabolism, and hemodynamics: application to the interpretation of functional neuroimaging. NeuroImage 17, 1162–1181.

Baillet, S., Mosher, J.C., Leahy, R.M., 2001. Electromagnetic brain mapping. IEEE Signal Process. Mag. 14–30.

Chawla, D., Friston, K.J., Lumer, E.D., 2001. Zero-lag synchronous dynamics in triplets of interconnected cortical areas. Neural Netw. 14, 727–735.

Clifford Carter, G., 1987. Coherence and time delay estimation. Proc. IEEE 75, 236–255.

David, O., Garnero, L., Cosmelli, D., Varela, F.J., 2002. Estimation of neural dynamics from MEG/EEG cortical current density maps: application to the reconstruction of large-scale cortical synchrony. IEEE Trans. Biomed. Eng 49, 975–987.

Engel, A.K., Fries, P., Singer, W., 2001. Dynamic predictions: oscillations and synchrony in top-down processing. Nat. Rev. Neurosci. 2, 704–716.

Frackowiak, R.S.J., Friston, K.J., Frith, C.D., Dolan, R.J., Mazziotta, J.C., 1997. Human Brain Function. Academic Press, San Diego.

Freeman, W.J., 1978. Models of the dynamics of neural populations. Electroencephalogr. Clin. Neurophysiol. [Suppl.] 34, 9–18.

Freeman, W.J., 1987. Simulation of chaotic EEG patterns with a dynamic model of the olfactory system. Biol. Cybern. 56, 139–150.

Friston, K.J., 2002. Bayesian estimation of dynamical systems: an application to fMRI. NeuroImage 16, 513–530.

Friston, K.J., Buechel, C., Fink, G.R., Morris, J., Rolls, E., Dolan, R.J., 1997. Psychophysiological and modulatory interactions in neuroimaging. NeuroImage 6, 218–229.

Friston, K.J., Penny, W., Phillips, C., Kiebel, S., Hinton, G., Ashburner, J., 2002. Classical and Bayesian inference in neuroimaging: theory. NeuroImage 16, 465–483.

Haskell, E., Nykamp, D.Q., Tranchina, D., 2001. Population density methods for large-scale modelling of neuronal networks with realistic synaptic kinetics: cutting the dimension down to size. Network 12, 141–174.

Honeycutt, R.L., 1992. Stochastic Runge-Kutta algorithms. I. White noise. Phys. Rev. A 45, 600–603.

Horwitz, B., Tagamets, M.A., 1999. Predicting human functional maps with neural net modeling. Hum. Brain Mapp. 8, 137–142.

Jansen, B.H., Rit, V.G., 1995. Electroencephalogram and visual evoked potential generation in a mathematical model of coupled cortical columns. Biol. Cybern. 73, 357–366.

Jefferys, J.G., Traub, R.D., Whittington, M.A., 1996. Neuronal networks for induced "40 Hz" rhythms. Trends Neurosci. 19, 202–208.

Jirsa, V.K., Haken, H., 1997. A derivation of a macroscopic field theory of the brain from the quasi-microscopic neural dynamics. Physica D 99, 503–526.

Lachaux, J.-P., Rodriguez, E., Martinerie, J., Varela, F.J., 1999. Measuring phase synchrony in brain signals. Hum. Brain Mapp. 8, 194–208.

Lopes da Silva, F.H., Hoeks, A., Smits, H., Zetterberg, L.H., 1974. Model of brain rhythmic activity. The alpha-rhythm of the thalamus. Kybernetik 15, 27–37.

Lopes da Silva, F.H., Pijn, J.P., Velis, D., Nijssen, P.C., 1997. Alpha rhythms: noise, dynamics and models. Int. J. Psychophysiol. 26, 237–249.

Lumer, E.D., Edelman, G.M., Tononi, G., 1997. Neural dynamics in a model of the thalamocortical system. II. The role of neural synchrony tested through perturbations of spike timing. Cereb. Cortex 7, 228–236.

Nunez, P.L., 1974. The brain wave equation: a model for the EEG. Math. Biosci. 21, 279–297.

Nunez, P.L., 1981. Electric Fields of the Brain. Oxford University Press, New York.

Nunez, P.L., 2000. Toward a quantitative description of large-scale neocortical dynamic function and EEG. Behav. Brain Sci. 23, 371–398.

Pijn, J.P., Velis, D.N., Lopes da Silva, F.H., 1992. Measurement of interhemispheric time differences in generalised spike-and-wave. Electroencephalogr. Clin. Neurophysiol. 83, 169–171.

Robinson, P.A., Rennie, C.J., Wright, J.J., Bahramali, H., Gordon, E., Rowe, D.L., 2001. Prediction of electroencephalographic spectra from neurophysiology. Phys. Rev. E 63, 021903.

Rodriguez, E., George, N., Lachaux, J.P., Martinerie, J., Renault, B., Varela, F.J., 1999. Perception's shadow: long-distance synchronization of human brain activity. Nature 397, 430–433.

Roelfsema, P.R., Engel, A.K., Konig, P., Singer, W., 1997. Visuomotor integration is associated with zero time-lag synchronization among cortical areas. Nature 385, 157–161.

Roulston, M.S., 1999. Estimating the errors on measured entropy and mutual information. Physica D 125, 285–294.

Stam, C.J., Pijn, J.P., Suffczynski, P., Lopes da Silva, F.H., 1999. Dynamics of the human alpha rhythm: evidence for non-linearity. Clin. Neurophysiol. 110, 1801–1813.

Stam, C.J., van Dijk, B.W., 2002. Synchronization likelihood: an unbiased measure of generalized synchronization in multivariate data sets. Physica D 163, 236–251.

Steriade, M., 2001. Impact of network activities on neuronal properties in corticothalamic systems. J. Neurophysiol. 86, 1–39.

Suffczynski, P., Kalitzin, S., Pfurtscheller, G., Lopes da Silva, F.H., 2001. Computational model of thalamo-cortical networks: dynamical control of alpha rhythms in relation to focal attention. Int. J. Psychophysiol. 43, 25–40.

Tass, P., Wienbruch, C., Weule, J., Kurths, J., Pikovsky, A., Volkmann, J., Schnitzler, A., Freund, H.-J., 1998. Detection of *n:m* phase locking from noisy data: application to magnetoencephalography. Phys. Rev. Lett. 81, 3291–3294.

Tononi, G., Sporns, O., Edelman, G.M., 1994. A measure for brain complexity: relating functional segregation and integration in the nervous system. Proc. Natl. Acad. Sci. USA 91, 5033–5037.

Valdes, P.A., Jimenez, J.C., Riera, J., Biscay, R., Ozaki, T., 1999. Nonlinear EEG analysis based on a neural mass model. Biol. Cybern. 81, 415–424.

Varela, F., Lachaux, J.-P., Rodriguez, E., Martinerie, J., 2001. The brainweb: phase synchronization and large-scale integration. Nat. Rev. Neurosci. 2, 229–239.

von Stein, A., Sarnthein, J., 2000. Different frequencies for different scales of cortical integration: from local gamma to long range alpha/theta synchronization. Int. J. Psychophysiol. 38, 301–313.

Wendling, F., Bartolomei, F., Bellanger, J.J., Chauvel, P., 2002. Epileptic fast activity can be explained by a model of impaired GABAergic dendritic inhibition. Eur. J. Neurosci. 15, 1499–1508.

Wendling, F., Bellanger, J.J., Bartolomei, F., Chauvel, P., 2000. Relevance of nonlinear lumped-parameter models in the analysis of depth-EEG epileptic signals. Biol. Cybern. 83, 367–378.

Whittington, M.A., Faulkner, H.J., Doheny, H.C., Traub, R.D., 2000b. Neuronal fast oscillations as a target site for psychoactive drugs. Pharmacol. Ther. 86, 171–190.

Whittington, M.A., Traub, R.D., Kopell, N., Ermentrout, B., Buhl, E.H., 2000a. Inhibition-based rhythms: experimental and mathematical observations on network dynamics. Int. J. Psychophysiol. 38, 315–336.

Wilson, H.R., Cowan, J.D., 1972. Excitatory and inhibitory interactions in localized populations of model neurons. Biophys. J. 12, 1–24.